

Single Site Isomeric Ru WOCs with an Electron Withdrawing Group: Synthesis, Electrochemical Characterization and Reactivity

Lorenzo Mognon,^a Jordi Benet-Buchholz,^a and Antoni Llobet^{,a,b}*

^a Institute of Chemical Research of Catalonia (ICIQ), Avinguda Països Catalans 16, 43007

Tarragona, Spain

^b Departament de Química, Universitat Autònoma de Barcelona, Cerdanyola del Vallès, 08193

Barcelona, Spain

ABSTRACT. The synthetic intermediate *cis(out),cis*-[Ru(Cl)₂(HL)(dmsO)₂], **1**, and four new mononuclear ruthenium complexes with general formula *out/in*-[Ru(HL)(trpy)(X)]^{m+} (X = Cl⁻, m = 1, **2a**⁺ and **2b**⁺; X = H₂O, m = 2, **3a**²⁺ and **3b**²⁺) based on the ligand 1*H*-Pyrazole-3-Carboxylic Acid, 5-(2-pyridinyl)-, ethyl ester (HL), are synthesized and characterized by analytical, spectroscopic and electrochemical methods. A linkage isomerism is observed for a dmsO moiety of **1**, and relevant thermodynamic and kinetic values are obtained through electrochemical experiments and compared to literature. Different synthetic routes are developed to obtain isomeric **2a**⁺ and **2b**⁺, with different relative yields. Water oxidation activity of **3a**²⁺ and **3b**²⁺ is analyzed by means of electrochemical methods, through foot-of-the-wave analysis, yielding *k*_{obs} values of 1.00 and 2.23 s⁻¹, respectively. Chemically driven water oxidation activity is tested using [(NH₄)₂Ce(NO₃)₆] as sacrificial electron acceptor, and values of TON = 10.8 and TOF_i = 58.2 × 10⁻³ s⁻¹ for **3a**²⁺ and TON = 4.2 and TOF_i = 15.4 × 10⁻³ s⁻¹ for **3b**²⁺ are obtained.

Introduction

Since the discovery by Thummel et al.¹ that mononuclear Ru complexes were active as catalysts for the water oxidation reaction, there has been a large development of the field based on this type of complexes.² A number of examples exist in the literature which are mainly based on the bipy³ and trpy-bpy⁴ systems. In 2008 Meyer et al.⁵ proposed a mechanistic description of how the water oxidation occurred at a molecular level: the O-O bond formation was proposed to occur based on the water nucleophilic attack pathway (WNA). This description has now been adapted to many other mononuclear Ru complexes, and also to some Ir or first row transition metals, where the water oxidation catalysis is claimed to proceed through a molecular pathway.⁶

Later on, Berlinguette and coworkers⁷ studied the strong influence that electronic perturbation of the metal center exerted through remote positions of the ligands over the whole water oxidation catalytic process. Our group have recently reported examples of mononuclear ruthenium terpy-bpy complexes having bpy substituted with fluoro groups at different positions, in order to observe the effect of electron withdrawing groups on the overall water oxidation process.⁸ Finally, recent reports by Yagi and coworkers⁹ have shown how the presence of a N-lone pair can influence reactivity in isomeric 2-(2-pyridyl)-1,8-naphthyridine complexes.

In the present work we report the full spectroscopic and electrochemical characterization of a new family of complexes of general formula *out/in*-[Ru(HL)(trpy)(X)]^{m+} (HL = 1H-Pyrazole-3-Carboxylic Acid, 5-(2-pyridinyl)-, ethyl ester; X = Cl⁻, m = 1, **2a**⁺ and **2b**⁺; X = H₂O, m = 2, **3a**⁺ and **3b**⁺), that allows to observe the subtle differences produced by the out and in constitutional isomers. These include specific intrinsic electronic trans and acid/base effects. Moreover, the

electron withdrawing nature of the ester will allow us to compare their performances with related complexes previously reported in the literature.

In addition we also report a synthetic intermediate with formula *cis(out)*, *cis*-[Ru(Cl)₂(HL)(dmsO)₂], **1**, that represents a new example of Ru-dmsO linkage isomerization phenomena prompted by a change in oxidation state of the Ru(II) metal center.

Experimental Section

Preparations. 1H-Pyrazole-3-Carboxylic Acid, 5-(2-pyridinyl)-, ethyl ester (HL),¹⁰ [RuCl₂(dmsO)₄]¹¹ and *cis*-[Ru(Cl)₂(trpy)(dmsO)]¹² were prepared accordingly to literature procedures.

***cis(out)*, *cis*-[Ru(Cl)₂(HL)(dmsO)₂]·H₂O, **1**·H₂O.** In a 250 mL round-bottom flask, HL (1.5 g, 6.91 mmol) and RuCl₂(dmsO)₄ (3.35 g, 6.91 mmol) are refluxed overnight in methanol (180 mL). The solution is then cooled to room temperature and a yellow solid is filtered. The solid is washed with cold methanol and with diethyl ether and then dried under vacuum. Yield: 2.525 g (67.0%). Anal. Calcd for C₁₅H₂₃Cl₂N₃O₄RuS₂·H₂O; C, 31.97; H, 4.47; N, 7.46; S, 11.38. Found: C, 32.23; H, 4.21; N, 7.32; S, 11.48. ¹H NMR (400 MHz, *d*₆-dmsO): δ = 9.23 (d, ³J₁₋₂ = 5.24 Hz, H1), 8.38 (d, ³J₄₋₃ = 7.74 Hz, H4), 8.21 (dd, ³J₃₋₄ = 7.74 Hz, ³J₃₋₂ = 7.74 Hz, H3), 7.97 (s, H7), 7.70 (dd, ³J₂₋₃ = 7.74 Hz, ³J₂₋₁ = 5.24 Hz, H2), 4.40 (m, H10), 3.47 (s, CH₃ of C14 and C15), 3.44 (s, H12), 2.54 (s, H13), 1.34 (t, ³J₁₁₋₁₀ = 7.11 Hz, H11). Cyclic voltammetry (CH₂Cl₂, TBAH): *E*_{1/2} = 1.39 V (Δ*E* = 121 mV).

***out*-[Ru(Cl)(HL)(trpy)](PF₆)·CH₃OH, **2a**(PF₆)·MeOH, and *in*-[Ru(Cl)(HL)(trpy)](PF₆)·H₂O, **2b**(PF₆)·H₂O. Route A.** In a 250 mL round bottom flask, **1** (200 mg, 0.367 mmol) and terpyridine (86 mg, 0.369 mmol) are dissolved in methanol (150 mL). The

solution is refluxed overnight. The mixture is then evaporated to dryness, and the resulting solid dissolved in CH_2Cl_2 and purified over neutral alumina using a mixture $\text{CH}_2\text{Cl}_2/\text{CH}_3\text{CN}$ (1:1, v/v) as eluent. The first pink fraction, corresponding to the out isomer, is added to 1 mL of a saturated aqueous NH_4PF_6 solution and then dried at the rotary evaporator. The residue thus obtained is dissolved in acetone and water is added. The acetone is evaporated until a brown solid precipitates. The solid is filtered on a frit, washed with cold water and diethyl ether and dried under vacuum. Yield: 161 mg (59.9%). Anal. Calcd for $\text{C}_{26}\text{H}_{22}\text{ClF}_6\text{N}_6\text{O}_2\text{PRu}\cdot\text{MeOH}$: C, 42.45; H, 3.43; N, 11.00. Found: C, 42.29; H, 3.15; N, 10.80. ^1H NMR (500 MHz, d_6 -acetone): δ = 10.18 (d, $^3J_{16-17}$ = 5.02 Hz, H16), 8.66 (d, $^3J_{7-8}$ = $^3J_{9-8}$ = 8.01 Hz, H7, H9), 8.63 (d, $^3J_{19-18}$ = 7.90 Hz, H19), 8.60 (d, $^3J_{4-3}$ = $^3J_{12-13}$ = 7.79 Hz, H4, H12), 8.35 (dd, $^3J_{18-19}$ = 7.90 Hz, $^3J_{18-17}$ = 7.66 Hz, H18), 8.15 (t, $^3J_{8-7}$ = $^3J_{8-9}$ = 8.01 Hz, H8), 8.01 (dd, $^3J_{3-4}$ = $^3J_{13-12}$ = 7.79 Hz, $^3J_{3-2}$ = $^3J_{13-14}$ = 7.57 Hz, H3, H13), 7.93 (dd, $^3J_{17-18}$ = 7.66 Hz, $^3J_{17-16}$ = 5.02 Hz, H17), 7.83 (d, $^3J_{1-2}$ = $^3J_{15-14}$ = 5.14 Hz, H1, H15), 7.80 (s, H22), 7.42 (dd, $^3J_{2-3}$ = $^3J_{14-13}$ = 7.57 Hz, $^3J_{2-1}$ = $^3J_{14-15}$ = 5.14 Hz, H2, H14), 4.40 (q, $^3J_{25-26}$ = 7.05 Hz, H25), 1.34 (t, $^3J_{26-25}$ = 7.05 Hz, H26). ESI-MS (MeOH): m/z = 587.0 ($[\text{Ru}(\text{Cl})(\text{HL})(\text{trpy})]^+$). Cyclic Voltammetry (CH_2Cl_2 , TBAH): $E_{1/2}$ = 1.04 V (ΔE = 95 mV).

The fraction remaining on the column, which corresponds to the in isomer together with $[\text{Ru}(\text{trpy})_2]^{2+}$ and other secondary products, is eluted with methanol and purified over a silica column using a solution 0.05 % of NH_4OH in methanol as eluent. The first yellow eluted fraction from this second column is discarded and the second one (purple) corresponds to the deprotonated in complex. This solution is evaporated to dryness and afterward dissolved in acetone containing a few drops of 0.5 M HCl and 1 mL of a saturated NH_4PF_6 aqueous solution.

Traces of silica are removed by filtration over cotton. The volume is then again reduced on a rotary evaporator until a solid precipitates out of the solution. The mixture is then cooled in a fridge overnight and the solid filtered on a frit, washed with cold water and diethyl ether, and dried under vacuum. Yield: 16 mg (6.0%) Anal. Calcd for $C_{26}H_{22}ClF_6N_6O_2PRu \cdot H_2O$: C, 41.64; H, 3.23; N, 11.21. Found : C, 41.59; H, 3.14; N, 11.15. 1H NMR (500 MHz, d_6 -acetone): δ = 8.74 (d, $^3J_{7-8} = ^3J_{9-8} = 8.05$ Hz, H7, H9), 8.62 (d, $^3J_{4-3} = ^3J_{12-13} = 7.98$ Hz, H4, H12), 8.35 (d, $^3J_{19-18} = 7.75$ Hz, H19), 8.22 (t, $^3J_{8-7} = ^3J_{8-9} = 8.05$ Hz, H8), 8.21 (s, H22), 8.02 (d, $^3J_{1-2} = ^3J_{15-14} = 5.39$ Hz, H1, H15), 8.01 (dd, $^3J_{3-4} = ^3J_{13-12} = 7.98$ Hz, $^3J_{3-2} = ^3J_{13-14} = 7.90$ Hz, H3, H13), 7.79 (dd, $^3J_{18-19} = 7.75$ Hz, $^3J_{18-17} = 7.60$ Hz, H18), 7.74 (dd, $^3J_{2-3} = ^3J_{14-13} = 7.90$ Hz, $^3J_{2-1} = ^3J_{14-15} = 5.39$ Hz, H2, H14), 7.45 (d, $^3J_{16-17} = 5.84$ Hz, H16), 7.02 (dd, $^3J_{17-18} = 7.60$ Hz, $^3J_{17-16} = 5.84$ Hz, H17), 4.55 (q, $^3J_{25-26} = 7.03$ Hz, H25), 1.47 (t, $^3J_{26-25} = 7.03$ Hz, H26). ESI-MS (MeOH): m/z = 587.1 ($[Ru(Cl)(HL)(trpy)]^+$). Cyclic Voltammetry (CH_2Cl_2 , TBAH): $E_{1/2} = 1.13$ V ($\Delta E = 144$ mV).

Route B. In a 250 mL round-bottom flask, *cis*- $[Ru(Cl)_2(dmsO)(trpy)]$ (177.4 mg, 0.367 mmol) and HL (80.0 mg, 0.368 mmol) are dissolved in methanol (150 mL) and the solution is refluxed for 5 days. The purification method is the same as route A. Yields: 32 mg of **2a** (11.9%) and 65 mg of **2b** (24.2%).

out- $[Ru(HL)(trpy)(H_2O)](ClO_4)_2 \cdot 2H_2O$, **3a $(ClO_4)_2 \cdot 2H_2O$.** In a 25 mL round-bottom flask, 50 mg (0.068 mmol) of *out*- $[Ru(Cl)(HL)(trpy)](PF_6)$ and 15 mg (0.072 mmol) of $AgClO_4$ are dissolved in 20 mL of a water/acetone 1:3 mixture and refluxed for 2 h away from light. The solution is then cooled in the fridge for 1h. The precipitated $AgCl$ is filtered over Celite. A few drops of a saturated $LiClO_4$ aqueous solution are added to the filtrate, and then the volume is reduced until the formation of a precipitate. The solution is then cooled in fridge overnight,

filtered and the solid washed with cold water and diethyl ether and then vacuum dried. Yield: 41 mg (78.5%). Anal. Calcd for $C_{26}H_{24}Cl_2N_6O_{11}Ru \cdot 0.5H_2O$: C, 40.17; H, 3.24; N, 10.81. Found: C, 40.05; H, 2.91; N, 10.62. 1H NMR (500 MHz, pD = 1.0 in 0.1 M CF_3SO_3D in D_2O): δ = 9.38 (d, $^3J_{16-17}$ = 5.52 Hz, H16), 8.50 (d, $^3J_{7-8}$ = $^3J_{9-8}$ = 8.15 Hz, H7, H9), 8.39 (d, $^3J_{12-13}$ = $^3J_{4-3}$ = 8.03 Hz, H12, H4), 8.36 (d, $^3J_{19-18}$ = 7.93 Hz, H19), 8.25 (dd, $^3J_{18-19}$ = 7.93 Hz, $^3J_{18-17}$ = 7.67 Hz, H18), 8.16 (t, $^3J_{8-7}$ = $^3J_{8-9}$ = 8.15 Hz, H8), 7.94 (dd, $^3J_{3-4}$ = $^3J_{13-12}$ = 8.03 Hz, $^3J_{3-2}$ = $^3J_{13-14}$ = 7.75 Hz, H3, H13), 7.86 (dd, $^3J_{17-18}$ = 7.67 Hz, $^3J_{17-16}$ = 5.52 Hz, H17), 7.75 (d, $^3J_{1-2}$ = $^3J_{15-14}$ = 5.55 Hz, H1, H15), 7.54 (s, H22), 7.29 (dd, $^3J_{2-3}$ = $^3J_{14-13}$ = 7.75 Hz, $^3J_{2-11}$ = $^3J_{14-15}$ = 5.55 Hz, H2, H14), 4.16 (q, $^3J_{25-26}$ = 7.15 Hz, H25), 1.15 (t, $^3J_{26-25}$ = 7.15 Hz, H26). ESI-MS (MeOH): m/z = 568.0 $[Ru(OH)(HL)(trpy)]^+$. Cyclic Voltammetry (pH = 1.0 in CF_3SO_3H): $E_{1/2}$ = 0.93 V (ΔE = 59 mV), $E_{1/2}$ = 1.26 V (ΔE = 165 mV); Cyclic Voltammetry (pH = 7.0 phosphate buffer): $E_{1/2}$ = 0.52 V (ΔE = 59 mV).

***in*-[Ru(HL)(trpy)(H₂O)](ClO₄)₂, **3b**(ClO₄)₂.** This compound is prepared following the same procedure as **3a**, but using complex **2b** instead of **2a** as reagent. Yield: 35.0 mg (67.0%). Anal. Calcd for $C_{26}H_{24}Cl_2N_6O_{11}Ru$: C, 40.64; H, 3.15; N, 10.94. Found: C, 40.52; H, 2.89; N, 10.66. 1H NMR (500 MHz, pD = 1.0 in 0.1 M CF_3SO_3D in D_2O): δ = 8.54 (d, $^3J_{19-18}$ = $^3J_{19-20}$ = 8.15 Hz, H19), 8.40 (d, $^3J_{15-14}$ = $^3J_{23-24}$ = 7.87 Hz, H15, H23), 8.20 (t, $^3J_{19-18}$ = $^3J_{19-20}$ = 8.15 Hz, H19), 7.99 (d, $^3J_{4-3}$ = 7.68 Hz, H4), 7.97 (s, H7), 7.94 (dd, $^3J_{14-13}$ = $^3J_{24-25}$ = 7.89 Hz, $^3J_{14-15}$ = $^3J_{24-23}$ = 7.68 Hz, H14, H24), 7.86 (d, $^3J_{12-13}$ = $^3J_{26-25}$ = 5.14 Hz, H12, H26), 7.59 (dd, $^3J_{3-4}$ = 7.68 Hz, $^3J_{3-2}$ = 7.56 Hz, H3), 7.35 (dd, $^3J_{13-14}$ = $^3J_{25-24}$ = 7.89 Hz dd, $^3J_{13-12}$ = $^3J_{25-26}$ = 5.49 Hz, H13, H25), 7.18 (d, $^3J_{1-2}$ = 5.49 Hz, H1), 6.81 (dd, $^3J_{2-3}$ = 7.56 Hz, $^3J_{2-1}$ = 5.49 Hz, H2), 4.56 (q, $^3J_{10-11}$ = 7.10 Hz, H10), 1.47 (t, $^3J_{11-10}$ = 7.10 Hz, H11). ESI-MS (MeOH): m/z = 569.1 $[Ru(OH)(HL)(trpy)]^+$.

Cyclic Voltammetry (pH = 1.0 in 0.1 M CF₃SO₃H): $E_{1/2}$ = 1.00 V (ΔE = 63 mV); cyclic voltammetry (pH = 7.0 in phosphate buffer): $E_{1/2}$ = 0.60 V (ΔE = 60 mV).

Instruments and measurements. Electrochemical experiments were performed in a one-compartment three electrode cell, using glassy carbon working electrode (ϕ = 3 mm), platinum counter electrode (ϕ = 2 mm) and SSCE or Hg/HgSO₄ as reference electrodes in organic or aqueous solvents, respectively. All the potentials reported are referred to NHE.

UV–vis spectroscopy was performed on a Cary 50 (Varian) UV–vis spectrometer using 1 cm quartz cells.

Online manometric measurements were carried out on a Testo 521 differential pressure manometer with an operating range of 0.1–10 kPa and accuracy within 0.5% of the measurements. The manometer was coupled to thermostatic reaction vessels for dynamic monitoring of the headspace pressure above each reaction solution. The manometer’s secondary ports were connected to thermostatic reaction vessels containing the same solvents and headspace volumes as the sample vials. Each measurement for a reaction solution (2.0 mL) was performed at 298 K. Online mass spectrometry measurements of the evolved gas were performed on a Pfeiffer Omnistar GSD 301C mass spectrometer, in the same conditions as the manometric measurements. The NMR spectroscopy experiments were performed on Bruker Avance 400 and 500 Ultrashield NMR spectrometers.

X-ray Crystal Structure Determination. Crystals of **1** were obtained by slow cooling of a saturated methanol solution of the complex. Crystals of both **3a**²⁺ and **3b**²⁺ were obtained by slow cooling of saturated aqueous solutions. The measured crystals were prepared under inert conditions immersed in perfluoropolyether as protecting oil for manipulation.

Data collection: Crystal structure determination for **1** was carried out using a Bruker-Nonius diffractometer equipped with an APEX 2 4K CCD area detector, a FR591 rotating anode with MoK α radiation, Montel mirrors as monochromator and an Oxford Cryosystems low temperature device Cryostream 700 plus (T = -173 °C). Crystal structure determinations for **3a**²⁺ and **3b**²⁺ were carried out using a Apex DUO diffractometer equipped with a Kappa 4-axis goniometer, an APEX II 4K CCD area detector, a Microfocus Source E025 IuS using MoK α radiation, Quazar MX multilayer Optics as monochromator and an Oxford Cryosystems low temperature device Cryostream 700 plus (T = -173 °C). Full-sphere data collection was used with ω and φ scans. Programs used: Data collection APEX-2,¹³ data reduction Bruker Saint¹⁴ V/.60A and absorption correction SADABS.^{15,16}

Structure Solution and Refinement: Crystal structure solution was achieved using direct methods as implemented in SHELXTL¹⁷ and visualized using the program XP. Missing atoms were subsequently located from difference Fourier synthesis and added to the atom list. Least-squares refinement on F² using all measured intensities was carried out using the program SHELXTL. All non hydrogen atoms were refined including anisotropic displacement parameters.

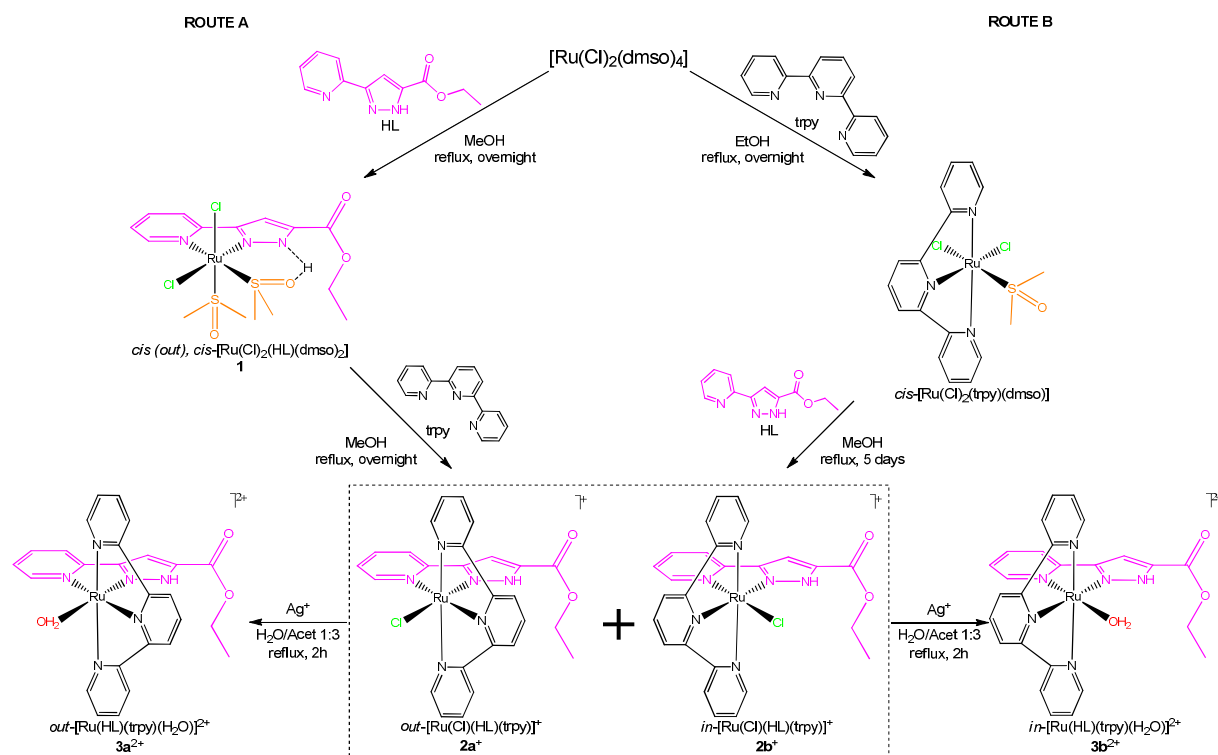
Comments to the structures: **1**: The asymmetric unit contains one molecule of the metal complex and one molecule of methanol. The methanol molecule is disordered in three orientations (ratio: 45:40:15). **3a**²⁺: The asymmetric unit contains one molecule of the ruthenium metal complex, two ClO₄ anions and two non-coordinated water molecules. One of the ClO₄ anions is disordered in two orientations (ratio: 60:40). **3b**²⁺: The asymmetric unit contains one molecule of the cationic metal complex and two ClO₄ anions.

Results and Discussion

Synthesis and solid state structure. The synthesis of the chlorido complexes **2a**⁺ and **2b**⁺ described in this work has been carried out by two different synthetic routes outlined in Scheme 1, that use [Ru(Cl)₂(dmsO)₄], as the starting material.

These two routes differ in the sequential substitution of the Cl and dmsO ligands by trpy and HL. In Route A, HL is refluxed in methanol together with [Ru(Cl)₂(dmsO)₄] to generate *cis(out)*, *cis*-[Ru(Cl)₂(HL)(dmsO)₂], **1**, which has an intense yellow color and where two dmsO ligands have been replaced by HL with a good isolated yield of over 67%. This substitution can potentially lead to the formation of six different stereoisomers, with two pairs of enantiomers, depending on the different relative coordination position of the chlorido and dmsO ligands.¹⁸

Scheme 1. Synthetic strategy and labelling scheme used for the ligands and complexes described in this work.



The predominance of **1** can be rationalized based on the synergic π -donor and π -acceptor capacities of the Cl and dmsO ligands when they are trans to one another, and the stabilization provided by the hydrogen bond between the pyrazole N-H and the oxygen atom of the equatorial dmsO ligand (see X-ray structure in Figure 1). Further reaction of **1** with trpy replaces one chlorido and two dmsO ligands to form a mixture of the *in* and *out* isomers $[\text{Ru}(\text{Cl})(\text{HL})(\text{trpy})]^+$, **2a⁺** and **2b⁺** in a 10:1 ratio. The two isomers can be easily separated by column chromatography first in alumina and then in silica, giving highly pure **2a⁺** and **2b⁺** with isolated yields of 60% and 6% respectively. In Route B, the trpy ligand is used in the first step, and upon reacting with $[\text{Ru}(\text{Cl})_2(\text{dmsO})_4]$ generates $\text{cis-}[\text{Ru}(\text{Cl})_2(\text{trpy})(\text{dmsO})]$ (that has been previously described),¹² and

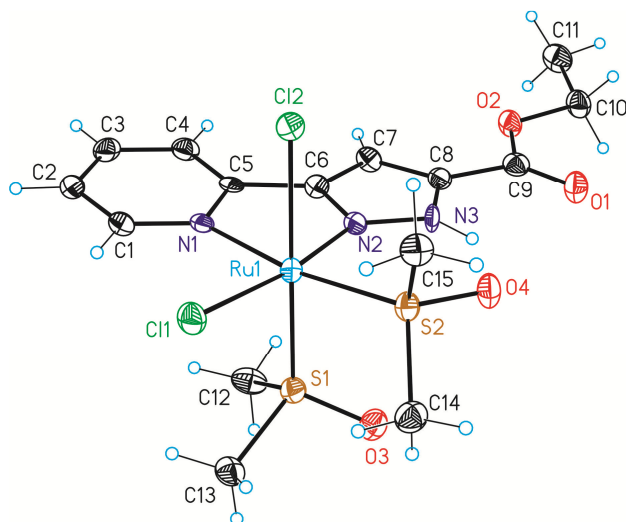
further addition of HL generates a mixture of the Ru-Cl isomer **2a**⁺ and **2b**⁺ in 12% and 24% yields respectively that represents a 1:2 ratio.

The different relative ratios of **2a**⁺ and **2b**⁺ obtained depending on the synthetic route clearly point out to the existence of strongly differentiating factors. In route A, it is clear that the replacement of 2 dmso and 1 Cl[−] of **1** by trpy takes place easily, forming directly **2a**⁺. On the other hand, for the **2b**⁺ case, an additional ligand reorganization is needed, otherwise the simple meridional substitution would generate *in*-[Ru(HL)(trpy)(dmso)]²⁺, that is not even detected. In sharp contrast, *cis*-[Ru(Cl)₂(trpy)(dmso)] shows a symmetry plane perpendicular to the trpy, and thus the differentiating factor comes from the relative orientation of the incoming HL ligand that will form a geometry with the chlorido ligand trans to the pyridyl nitrogen, thus favoring **2b**⁺, or to the pyrazolyl nitrogen, thus favoring **2a**⁺.

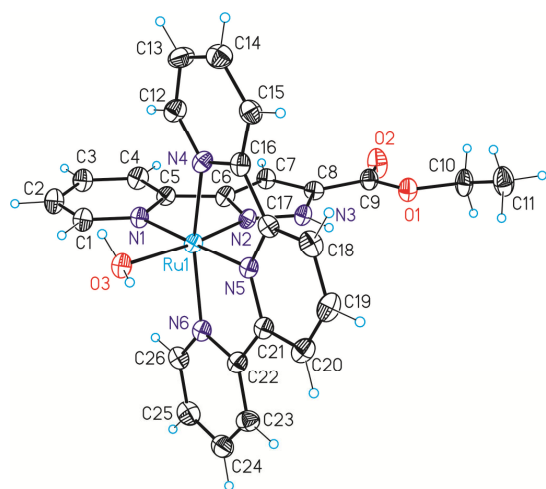
A 2 hours reflux of **2a**⁺, or **2b**⁺, in an acetone/water mixture in presence of AgClO₄ yields the aquo compounds **3a**²⁺ and **3b**²⁺, respectively, in good yields (79% and 67%). Light exposure (100 W tungsten lamp) of pure **3a**²⁺ or **3b**²⁺ in a 0.1 M CF₃SO₃D in D₂O for 14 hours produces an isomerization phenomenon that generates a 1:1 mixture of **3a**²⁺ and **3b**²⁺. This isomerization reaction was monitored by NMR spectroscopy and a 1:1 mixture is always obtained irrespectively of the starting material used, manifesting that both isomers have comparable stabilities (Figure S6).

Figure 1. ORTEP drawing (thermal ellipsoids 50 %) of complexes: (A) **1**, (B) **3a**²⁺, and (C) **3b**²⁺.

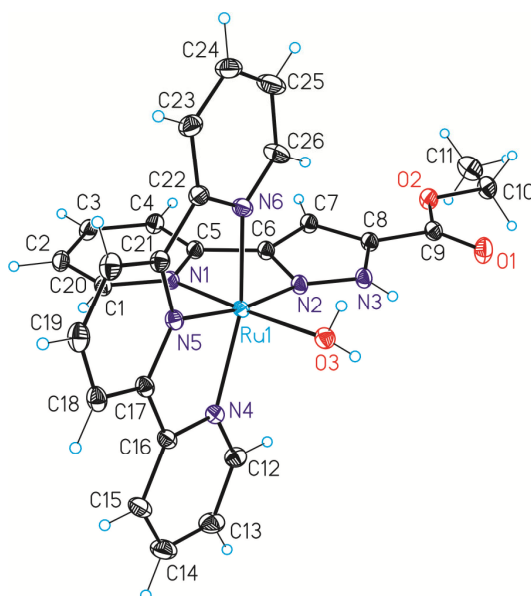
A



B



C



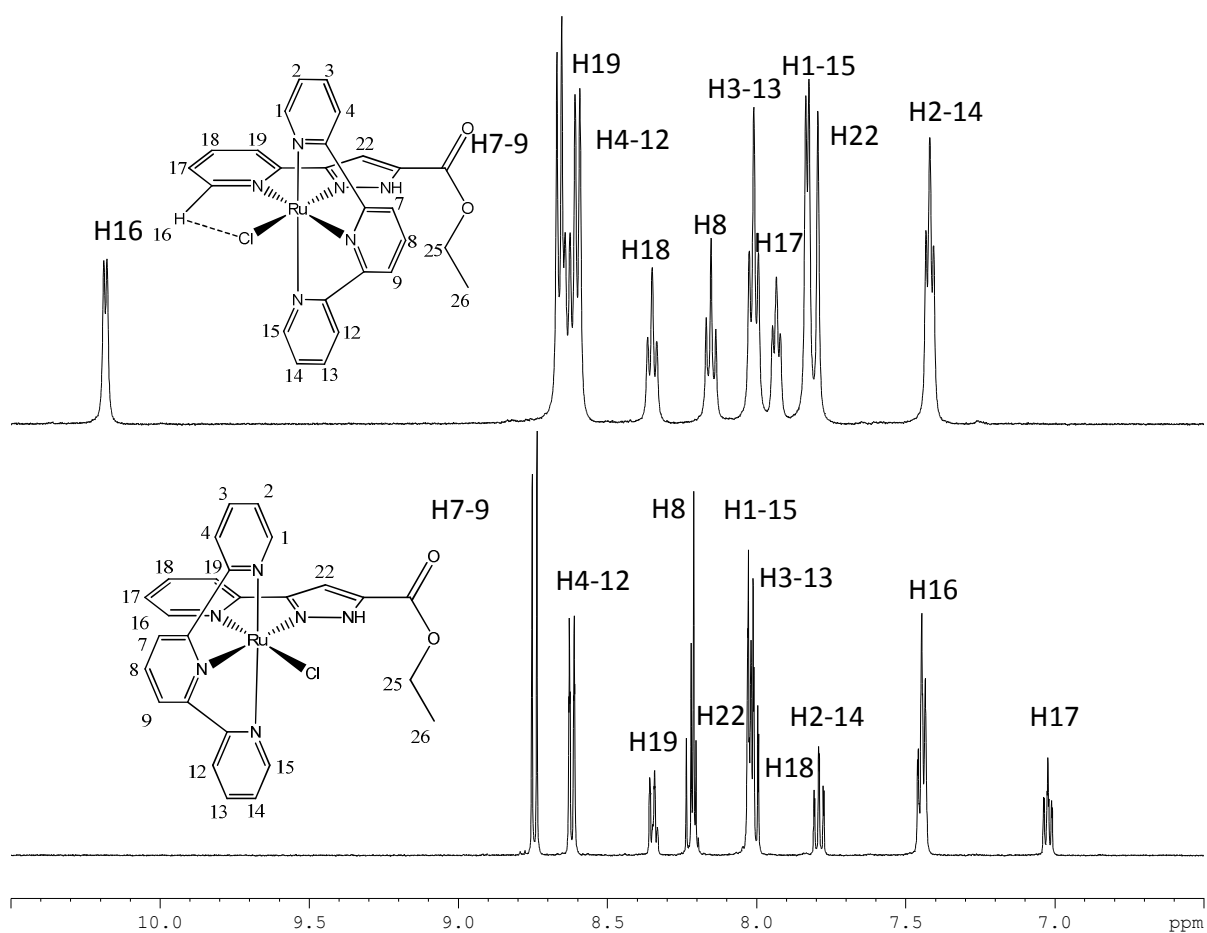
Monocrystals for complexes **1**, **3a**²⁺ and **3b**²⁺ were obtained and their crystal structures solved by means of X-ray diffraction analysis. An ORTEP drawing for **1**, **3a**²⁺ and **3b**²⁺ is shown in Figure 1. In all the structures the geometry around the metal center consists of a distorted octahedron as expected for a low-spin d⁶ Ru(II), similar to previously reported complexes.^{8, 19} It is interesting to mention that complex **1** presents a strong hydrogen bonding between H3A and O4 (N(3)-H(3A) = 0.0881(3) Å, H(3A)-O(4) = 2.044(3) Å, N(3)-O(4) = 2.746(5) Å, N(3)-H(3A)-O(4) = 135.9(2)°).

Spectroscopic properties. ¹H NMR, COSY and NOESY of all the complexes were registered in d₆-dmsO, d₆-acetone or in pD = 1.0 CF₃SO₃D in D₂O, and are presented in Figure 2 and in the Supporting Information. All the resonances could be identified based on symmetry, integrations and thanks to bidimensional experiments and show that the structures described in the solid state are maintained in solution.

Complexes **2a**⁺, **2b**⁺, **3a**²⁺ and **3b**²⁺ possess a symmetry plane that contains the HL ligand and bisects the trpy ligand thus rendering the lower and upper protons of the pyridyl-trpy moieties magnetically equivalent. It is worth mentioning here that complex **2a**⁺ shows the typical signal at low field (δ = 10.18) for a proton deshielded due to the diamagnetic anisotropy generated by the chlorido ligand,²⁰ allowing one to fully assign the signals. A further clue in this direction is given by the NOE signal between H19 and H22 (2.30 Å, see Figure S2). None of these features are present in **2b**⁺ spectra, so its assignment is based on intensities of the integrals and experimental considerations on the coupling constants of pyridyl systems: the closer the proton to the nitrogen, the smaller the coupling constant. For complexes **3a**²⁺ and **3b**²⁺ the NMR was run in presence of ascorbic acid to avoid complex oxidation, and the same deshielding due to anisotropic effects,

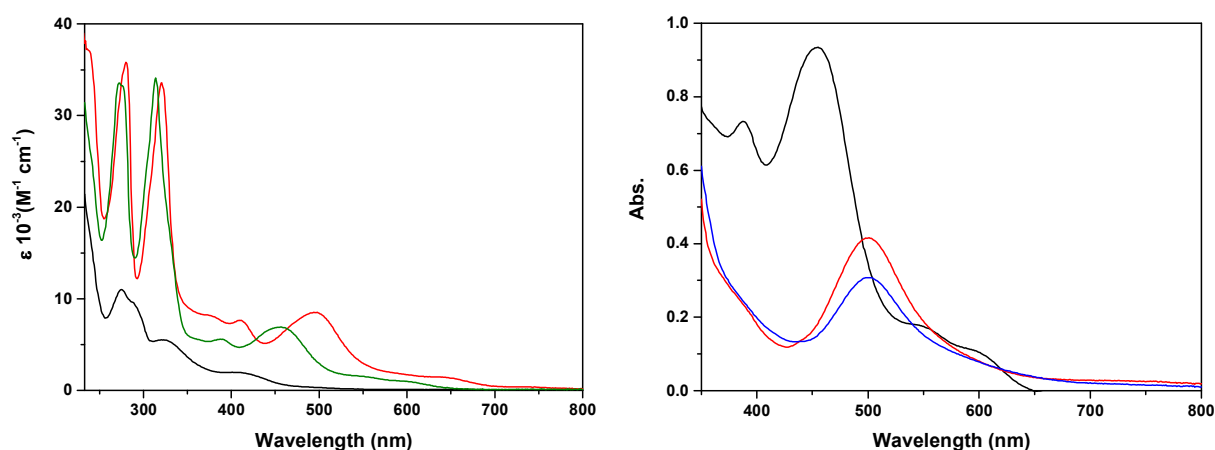
this time coming from the aqua ligand, can be seen in **3a**²⁺ for the signal of H16 ($\delta = 9.38$, Figure S4).

Figure 2. ¹H-NMR spectra in *d*₆-acetone (500 MHz, 298 K) and assignment for complexes (top) **2a**⁺ and (bottom) **2b**⁺.



The optical properties of the Ru-Cl complexes **1**, **2a**⁺ and **2b**⁺ were investigated by UV-vis spectroscopy in CH₂Cl₂ and those of the Ru-aqua complexes **3a**²⁺ and **3b**²⁺ were recorded in 0.1 M triflic acid aqueous solution and are displayed in Figure 3 and in the SI.

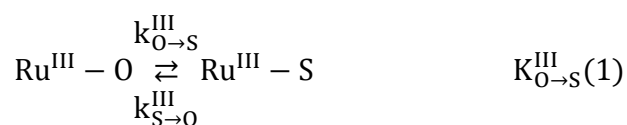
Figure 3. UV-vis spectra of (left) **1** (black) and **2a**⁺ (red) in CH₂Cl₂ and **3a**²⁺ (green) in a pH = 1 CF₃SO₃H solution.; and (right) different oxidation states of **3a**²⁺ in a pH = 1 CF₃SO₃H solution: Ru(II) (black), Ru(III) (red) and Ru(IV) (blue).



All the spectra show the typical π - π^* transitions due to the aromatic ligands below 350 nm, and weaker MLCT $d\pi$ - π^* between 400 and 650 nm. It is interesting to see the shift to lower energies of the Ru-Cl MLCT with regard to the Ru-OH₂ complexes due to a destabilization of the Ru $d\pi$ orbitals exerted by the chlorido ligand.^{19b, 21} The spectra of out and in isomers both in case of the chlorido and the aqua complexes are practically identical. Spectrophotometric redox titrations were also carried using Ce(IV) as oxidant for **3a**²⁺ and **3b**²⁺ and are displayed in Figure 3 and in the SI, respectively.

Redox properties of Ru-Cl complexes and linkage isomerization. The redox properties of the Ru-Cl complexes **1**, **2a**⁺ and **2b**⁺ presented in this work were analyzed by means of cyclic voltammetry in a solution 0.1 M of TBAH [(nBu₄N)(PF₆)] in CH₂Cl₂ and their redox potentials are referred to the NHE electrode. All CVs were run at a scan rate of 50 mV/s, unless explicitly stated. Glassy carbon electrodes were used as working electrodes and platinum electrodes as auxiliary electrodes.

The electrochemistry of complex **1** shows the typical behavior associated with a dmso ligand isomerization.^{18, 22} In the anodic scan, a wave (*i*_{a1}) can be seen at *E*_{p,a} = 1.42 V, with a cathodic wave (*i*_{c1}) at *E*_{p,c} = 1.33 V much less intense. A second cathodic wave *i*_{c2} is seen at *E*_{p,c} = 0.65 V. To fully understand this redox behavior, we performed quick Controlled Potential Electrolysis (CPE) at 0.24 V and at 1.84 V, followed by CVs at different scan rates. As can be seen in Figure 4, upon oxidation of the complex the waves at higher potentials diminish in intensity, while a new anodic wave *i*_{a2} rises at a lower potential of *E*_{p,a} = 0.76 V. The ratios [*i*_{c1}]/[*i*_{a1}] and [*i*_{c2}]/[*i*_{a2}] depend strongly on the scan rate. We associate this behavior with a different coordination mode of a dmso ligand, either S or O bond. The higher potential redox wave is associated to the Ru(III)/Ru(II) couple when the dmso is bonded through the S atom; when in oxidation state Ru(III), the metal center shows more affinity for the oxygen atom of the ligand, thus promoting the ligand isomerization. The O bonded dmso is a worse π-accepting ligand than the S bonded, so the redox potential for the Ru(III)/Ru(II) couple of the O bonded complex is lower. This equilibrium upon the one electron oxidation of **1** can be described as:



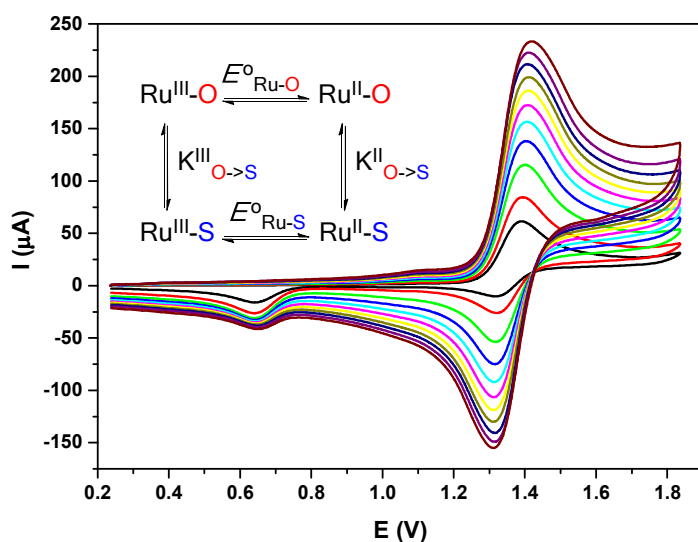
The equilibrium constant $K^{\text{III}}_{\text{O} \rightarrow \text{S}}$ for the $\text{Ru}^{\text{III}}\text{-O/Ru}^{\text{III}}\text{-S}$ reaction can be obtained from the CVs starting at 1.84 V, plotting the ratio $[i_{\text{c1}}]/[i_{\text{c2}}]$ versus the inverse of the scan rate (v^{-1} , see Figure S13c) and extrapolating for $v \rightarrow \infty$, where the intensities of the waves correspond to the concentrations at the equilibrium. This mathematical treatment results in $K^{\text{III}}_{\text{O} \rightarrow \text{S}} = 0.41$.

The kinetic constants for the isomerization were calculated using the working curves proposed by Shain and co-workers²³ for the case of a reversible chemical reaction preceding an electron transfer. The ratio i_k/i_d was calculated by measuring i_k (i_k is the measured peak current, i_{c1}) starting at 1.84 V after a CPE of 2 minutes, and i_d (i_d is the corresponding diffusion current in the absence of a chemical reaction, i_{a1}) starting at 0.24 V after a CPE of 2 minutes. The values thus obtained are: $k^{\text{III}}_{\text{O} \rightarrow \text{S}} = 2.0 \times 10^{-1} \text{ s}^{-1}$ and $k^{\text{III}}_{\text{S} \rightarrow \text{O}} = 4.9 \times 10^{-1} \text{ s}^{-1}$.

Assuming $E^0 = E_{1/2}$ and knowing the value of $K^{\text{III}}_{\text{O} \rightarrow \text{S}}$, the thermodynamic cycle in the inset of Figure 4 can be derived and used to calculate $K^{\text{II}}_{\text{S} \rightarrow \text{O}} = 2.1 \times 10^{+11}$.

The kinetic isomerization constant $k^{\text{II}}_{\text{O} \rightarrow \text{S}}$ can be extrapolated from the dependency of $\ln(i_{\text{a2}}/v^{1/2})$ vs. time²⁴ and yields a value of $9.3 \times 10^{-2} \text{ s}^{-1}$. The remaining constant can be obtained from the value of $K^{\text{II}}_{\text{S} \rightarrow \text{O}}$, resulting in $k^{\text{II}}_{\text{S} \rightarrow \text{O}} = 4.5 \times 10^{-13} \text{ s}^{-1}$.

Figure 4. (Top) Cyclic voltammograms at different scan rates obtained after 2 minutes CPE at an $E_{app} = 0.24$ V for a solution of **1** in 0.1M TBAH in CH_2Cl_2 . Black: 50 mV/s, red: 100 mV/s, green: 200 mV/s, blue: 300 mV/s, light blue: 400 mV/s, pink: 500 mV/s, yellow: 600 mV/s, dark yellow: 700 mV/s, dark blue: 800 mV/s, purple: 900 mV/s and brown: 1000 mV/s. Inset: linkage isomerization cycle for the Ru-dmso system, only the dmso atom bonded to the Ru metal center is shown. (Bottom) Plot of $K_{O \rightarrow S}^{III}$ versus $E_{1/2}(Ru-S)$ for a series of complexes reported in Table 1; the numbers correspond to the entry of Table 1.



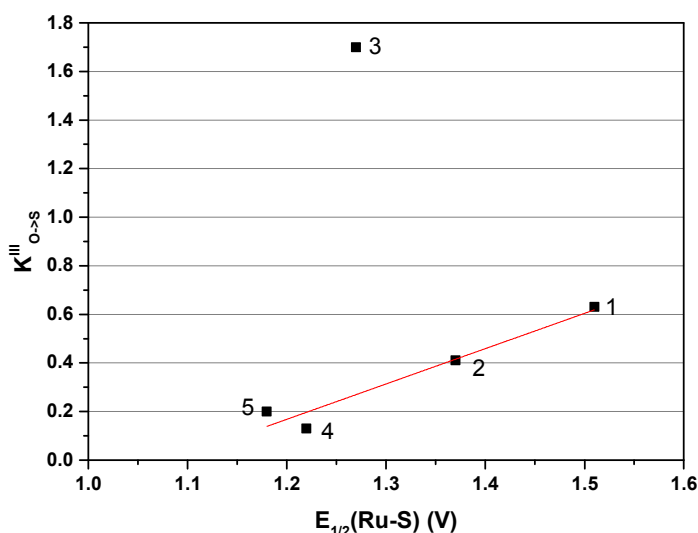


Table 1. Thermodynamic and kinetic data of selected complexes for comparison with complex 1.

Entry	Complex	$K_{O \rightarrow S}^{III}$	$k_{O \rightarrow S}^{III}$ [s ⁻¹]	$k_{S \rightarrow O}^{III}$ [s ⁻¹]	$K_{(O \rightarrow S)}^{II}$	$k_{O \rightarrow S}^{II}$ [s ⁻¹]	$k_{S \rightarrow O}^{II}$ [s ⁻¹]	$E_{1/2}$ (Ru-S) [V]	$E_{1/2}$ (Ru-O) [V]	Solv
1 ²⁴	<i>cis</i> , <i>cis</i> , <i>cis</i> - [Ru(Cl) ₂ (dmsO) ₂ (tbp) ₂]	0.63	1.2	1.9	$2.1 \times 10^{+12}$	1.0×10^{-2}	5.0×10^{-14}	1.51	0.79	MeCN
2	1	0.41	2.0×10^{-1}	4.9×10^{-1}	$2.1 \times 10^{+11}$	9.3×10^{-2}	4.5×10^{-13}	1.37	0.69	CH ₂ Cl ₂
3 ²²	<i>cis(out)</i> , <i>cis</i> - [Ru(Cl) ₂ (H3p)(dmsO) ₂]	1.7	2.8×10^{-1}	1.7×10^{-1}	$5.2 \times 10^{+11}$	4.9×10^{-1}	9.3×10^{-14}	1.27	0.70	CH ₂ Cl ₂
4 ²⁵	<i>out</i> - [Ru(dmsO)(Hbp)(trpy)] ⁺	0.13	7.7×10^{-2}	6.0×10^{-1}	$5.5 \times 10^{+8}$	2.5×10^{-1}	4.6×10^{-10}	1.22	0.65	CH ₂ Cl ₂
5 ²²	<i>trans</i> , <i>cis</i> - Ru(Cl) ₂ (H3p)(dmsO) ₂	0.20	5.7×10^{-2}	2.2×10^{-1}	$5.3 \times 10^{+8}$	8.7×10^{-2}	1.6×10^{-10}	1.18	0.63	CH ₂ Cl ₂

mso)₂]

The acronyms tbpy, bpp and H3p stand for the 4-*tert*-butylpyridine, the 3,5-(2-pyridyl)pyrazolato and the 5-phenyl-3-(2-pyridyl)-pyrazolato ligands respectively.

Table 1 compiles similar data for related Ru-dmso complexes reported in the literature that also undergo linkage isomerization processes as described by the square cycle shown in the inset of Figure 4. In general $K^{\text{II}}_{\text{O} \rightarrow \text{S}}$ are extremely high, meaning that once formed the Ru^{II}-O species immediately isomerizes towards Ru^{II}-S. On the other hand the tendency to isomerize for the Ru^{III}-S to the corresponding Ru^{III}-O, although generally favored, is much lower. It is interesting to observe in Table 1 that the K^{III} value nicely correlates with $E_{1/2}(\text{Ru-S})$ redox potential except for complex in entry 3 as can be seen graphically in Figure 4. This phenomenon can be rationalized in terms of the Pearson theory for hard and soft acids and bases (HSAB), where the higher the HOMO-LUMO gap the higher the hardness of a particular transition metal Lewis acid. In this sense the higher redox potential for the Ru(III)/Ru(II) couple would imply a lower energy for the d π orbitals and thus a larger HOMO-LUMO gap.

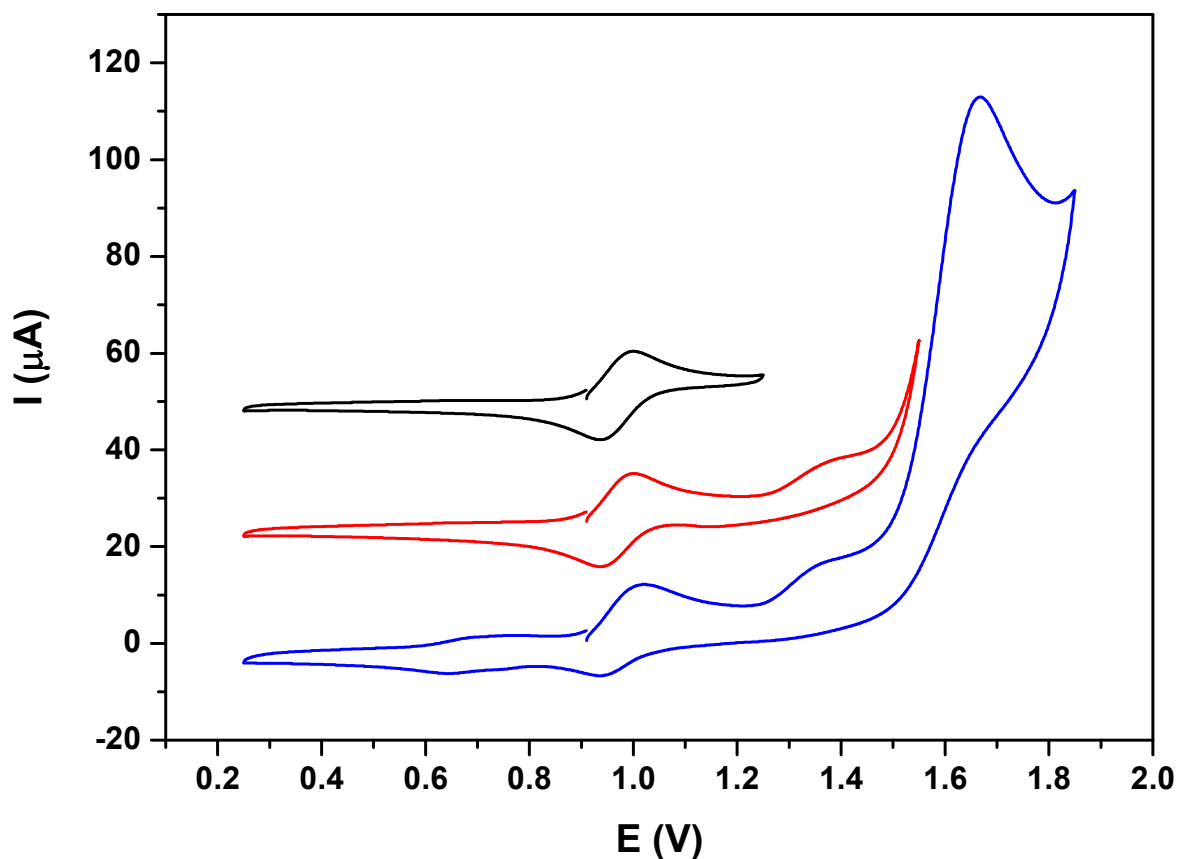
In CH₂Cl₂, complex **2a**⁺ shows a chemically reversible and electrochemically quasi-reversible wave at 1.04 V ($\Delta E = 95$ mV), while **2b**⁺ shows a chemically reversible and electrochemically irreversible wave at 1.13 V ($\Delta E = 144$ mV). Both waves can be assigned to the Ru(III)/Ru(II) couple, and the 90 mV potential difference between the two isomers is attributed to the different trans organization in the first coordination sphere of the metal center:^{19b} while the Ru-Cl bond is trans to N-pyrazole in **2a**⁺, in **2b**⁺ the Ru-Cl is trans to the N-pyridyl of the HL ligand.

Redox properties of Ru-H₂O complexes and water oxidation catalysis. The redox properties of the Ru-H₂O complexes **3a**²⁺ and **3b**²⁺ were analyzed by means of cyclic

voltammetry and differential pulse voltammetry in aqueous solutions, using 0.1 M CF₃SO₃H for the measurement at pH = 1.0 or the appropriate phosphate buffer for measurement at other pHs. Their redox potentials are referred to the NHE electrode.

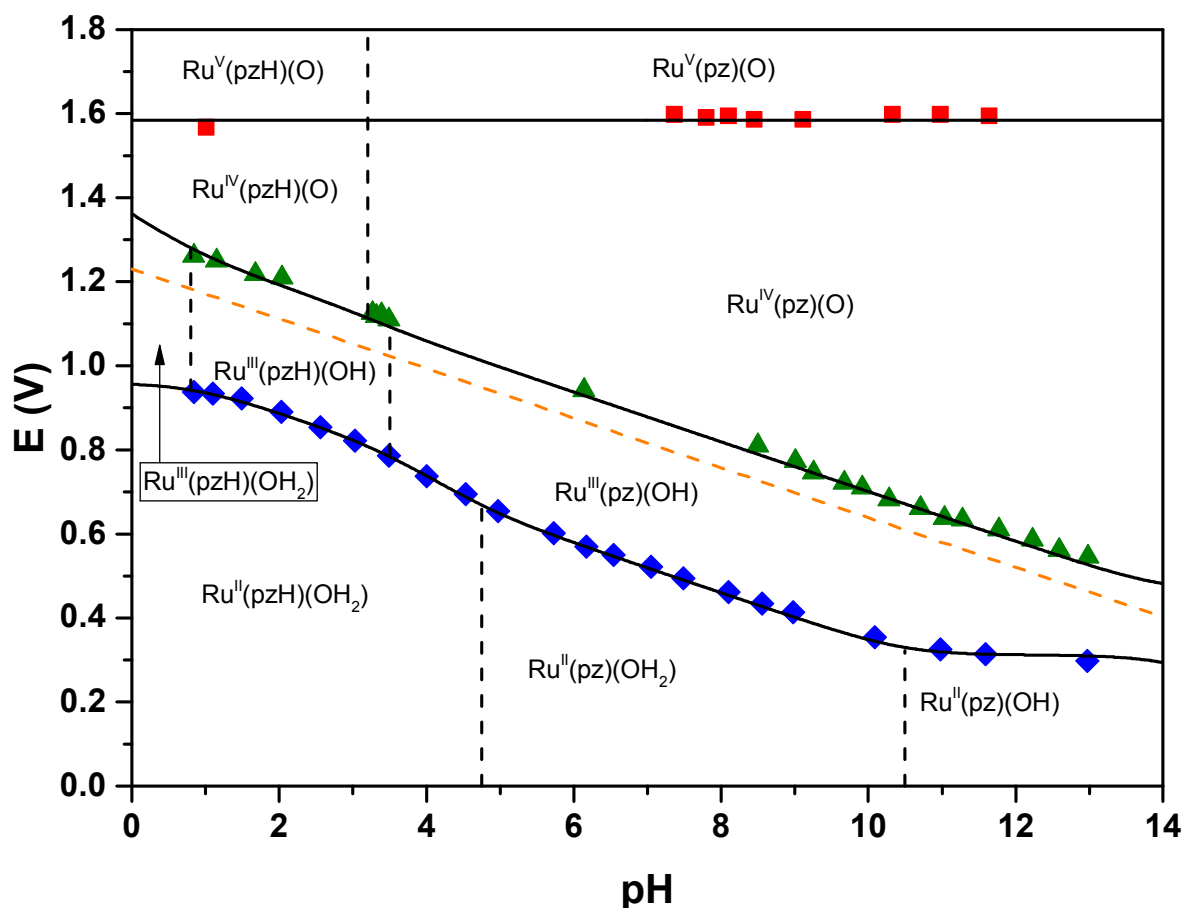
At pH = 1 complex **3a**²⁺ shows a chemical and electrochemical reversible wave at 0.93 V (ΔE = 59 mV), assigned to the Ru(III)/Ru(II) couple as can be seen in Figure 5. A second anodic waves assigned to the IV/III couple is observed at 1.35 V that has a very broad cathodic wave. The full recovery of the III/II wave in the cathodic region (i_a/i_c = 1.01) indicates the presence of slow ET process rather than a decomposition pathway. Further in the anodic region, a large electrocatalytic current intensity is observed whose foot of the wave is approximately at 1.5 V. After catalysis, in the reverse scan the IV/III wave is not observed at all and a small amount of the III/II is found (i_a/i_c = 2.42), clearly pointing out towards the existence of decomposition pathways coupled to the water oxidation reaction. Indeed further scanning in the cathodic region shows the presence of a new redox process with potential close to 0.65 V whose nature is unknown.

Figure 5. iR compensated CV of **3a**²⁺ in an aqueous pH = 1.0 CF₃SO₃H at a scan rate of 50 mV/s on glassy carbon electrode.



All the redox waves observed are pH dependent except for the V/IV wave as can be observed in the Pourbaix diagram displayed in Figure 6, where the zones of stability of the different species with different degree of oxidation and protonation derived from $3\mathbf{a}^{2+}$ are reported.

Figure 6. Pourbaix diagram for complex $3\mathbf{a}^{2+}$. pZH stands for the pyrazolic proton.



The pH dependency of the III/II and IV/III waves arises from the capacity of the aqua ligand directly bonded to Ru to undergo up to two proton losses and from the pyrazolato moiety of the HL ligand. All pK_a are represented with vertical lines in the Pourbaix diagram. For the III/II redox couple the evolution of the redox potential as function of pH is influenced by two deprotonation events at oxidation state II and two at oxidation state III and thus is rather complex. For this reason mathematical simulation was carried out using Equation 2:

$$E(\text{III/II}) = [E(\text{III/II})_{\text{pH}=0}] + \left(0.05916 * \log \left(\frac{[\text{H}^+]^3 + [\text{H}^+]^2 K_{a1}^{\text{II}} + [\text{H}^+] K_{a1}^{\text{II}} K_{a2}^{\text{II}} + K_{a1}^{\text{II}} K_{a2}^{\text{II}} K_{a3}^{\text{II}}}{[\text{H}^+]^3 + [\text{H}^+]^2 K_{a1}^{\text{III}} + [\text{H}^+] K_{a1}^{\text{III}} K_{a2}^{\text{III}} + K_{a1}^{\text{III}} K_{a2}^{\text{III}} K_{a3}^{\text{III}}} \right) \right) \quad (2)$$

where $E(\text{III/II})_{\text{pH}=0}$ is the potential for the III/II couple at pH = 0 and K_{an}^{X} is the n^{th} acid –base constant for the specie in oxidation state X.

This allowed us to extract the correct pK_{a} values that are reported in Table 2, along with other relevant thermodynamic and kinetic properties of complex $\mathbf{3a}^{2+}$ and other related complexes for comparison purposes. Although much simpler because of the lower number of pK_{a} involved the IV/III redox waves was also simulated and is also exhibited in the Pourbaix diagram.

For the case of the $\mathbf{3b}^{2+}$ isomer the electrochemical properties are relatively similar and the CVs and Pourbaix diagram are reported in the Supporting Information. One of the most striking features when comparing the two constitutional isomers is the value of $\Delta E_{1/2}$, defined as the difference between the IV/III and III/II redox potentials which is 360 mV for $\mathbf{3a}^{2+}$ and 240 for $\mathbf{3b}^{2+}$ at pH = 7.0. This manifests that for $\mathbf{3a}^{2+}$ the zone of stability of oxidation state III is much more favored than in the case of $\mathbf{3b}^{2+}$. This is necessarily an electronic effect produced by the different relative trans coordination of the HL ligand, as discussed in the structural section, and highlights how very small variations of the complex structure can strongly influence the electronic properties of the Ru metal center.

Comparing the redox potential of complex $\text{out-}[\text{Ru}(\text{Hbpp})(\text{trpy})(\text{H}_2\text{O})]^{2+}$ (Table 2, entry 1) ²¹ with $\mathbf{3a}^{2+}$, the electron withdrawing effect exerted by the carboxylate group can be clearly seen in an increment of 30 mV of the IV/III couple and of 40 mV for the III/II couple. In sharp contrast comparing it with $\mathbf{3b}^{2+}$, the latter increases the III/II by 130 mV but does not modify the IV/III redox potentials, again showing the difficulty of predicting beforehand the redox potentials of a particular redox couple. It is important to mention here that correlations have been

reported in the literature between redox potentials based on ligand electron donating and/or electron withdrawing effects, such as the ones proposed by Lever et al.²⁶ Those correlations are certainly useful and give a rough estimate of the potentials especially for those cases where only one oxidative ET is found within the limits of the solvent stability. In this case however, the calculations do not differentiate between isomers and thus manifest once more the need to prepare, separate and purify complexes undergoing multiple ET processes to measure their redox couples. As further example, it is interesting to see how electronic perturbation on the Ru(H₂O)-trpy-substituted-bpy system influence redox potentials when compared with unsubstituted bpy ligands (See entries 4-7 in Table 2). In particular, entry 5 presents an electron donating group, which should decrease the IV/III and III/II redox potentials, while entry 6 presents an electron withdrawing group, which in turn should increase the potentials. The effects are the expected ones, but to different extents on different redox couples, so that they generate in both cases an unexpected increase of the zone of stability of oxidation state III. In sharp contrast the electron withdrawing F-group in entry 7 produces just the opposite effect, wiping out the stability zone of the oxidation state II, and only a two-electron wave for the IV/II couple is found.

The electron withdrawing perturbation exerted by the carboxylate group is also obviously transmitted to the pK_a values of all the acid-base moieties of the complexes, namely the Ru-H₂O/Ru-OH couple and the pyrazolate/pyrazolato couple. Comparing Entry 1 with **3a**²⁺ a decrease of all pK_a values is observed, as expected. On the other hand, the potential hydrogen bonding between the Ru-OH₂, the proton from the pyrazolate moiety and a free water that could take place for the **3b**²⁺ isomer, but that cannot occur in **3a**²⁺, produces an increase of all the related pK_a values meaning that all the conjugated bases are stabilized by hydrogen bonding.

Table 2. Thermodynamic and catalytic data for **3a**²⁺ and **3b**²⁺ and for related Ru-aqua complexes described in the literature at pH = 7.0.

Entry	Complex ^a	$E_{1/2}$ (V) vs. NHE				ΔE^c	$pK_{a,II}^d$	$pK_{a,III}^d$	$pK_{a,III}^e$ pyrazole	TOF _i ·10 ³ (TON) ^f
		IV/III	III/II	IV/II ^b	V/IV					
1 ²¹	<i>out</i> -[Ru(Hbpp)(trpy)(H ₂ O)] ²⁺	0.85	0.48	0.67		370	11.1	2.8	6.88/5.43	
2	<i>out</i> - 3a ²⁺	0.88	0.52	0.70	1.59	360	10.5	0.8	4.75/3.5/3.2	58.2 (10.8)
3	<i>in</i> - 3b ²⁺	0.85	0.61	0.73	1.54	240	10.8	1.0	5.6/4.5/4.0	15.4 (4.2)
4 ⁸	[Ru(trpy)(bpy)(H ₂ O)] ²⁺	0.83	0.72	0.78	1.86	110	9.8	1.7		15.1 (18.3)
5 ⁷	[Ru(trpy)(4,4'-(MeO) ₂ -bpy)(H ₂ O)] ²⁺	0.82	0.64	0.76		240	11.2	3.2		
6 ⁷	[Ru(trpy)(4,4'-(HOOC) ₂ -bpy)(H ₂ O)] ²⁺	0.89	0.75	0.82		140	10.4	1.2		
7 ⁸	[Ru(trpy)(6,6'-F ₂ -bpy)(H ₂ O)] ²⁺	--	--	0.80 ^g	1.93	--	10.4	--		1.7 (7.8)

^aLigand abbreviations: 4,4'-(MeO)₂-bpy is 4,4'-dimethoxy-2,2'-bipyridine; 4,4'-(HOOC)₂-bpy is 4,4'-dicarboxy-2,2'-bipyridine. ^bCalculated as $[E(IV/III)+E(III,II)]/2$. ^c $\Delta E = E(IV/III)-E(III,II)$ in mV. ^d $pK_{a,II}$ and $pK_{a,III}$ represent the pK_a of the corresponding Ru^{II}-OH₂ and Ru^{III}-OH₂ species, respectively. ^e pK_a for the pyrazole proton, at the different oxidation states II/III/IV. ^fTOF_i stands for initial Turn Over Frequencies in cycles per second and TON for Turn Over Numbers. This values are extracted for the catalytic reactions involving 1.0 mM Cat/100 mM Ce(IV) in a 0.1 M triflic acid solution with a total volume of 2 mL. ^gTwo electron process.

In order to obtain kinetic information about the catalytic process, a “foot of the wave analysis” was carried out to calculate apparent rate constant k_{obs} . We followed the methodology described

by Saveant et al.²⁷ which assumes that the rate determining step (rds) is the last electron transfer.

Under catalytic conditions Equation 3 is operative,

$$\frac{i}{i_p^0} = \frac{8.96 \sqrt{\frac{RT}{Fv}} k_{\text{obs}}}{1 + \exp \left[\frac{F}{RT} (E_{\text{PQ}}^0 - E) \right]} \quad (3)$$

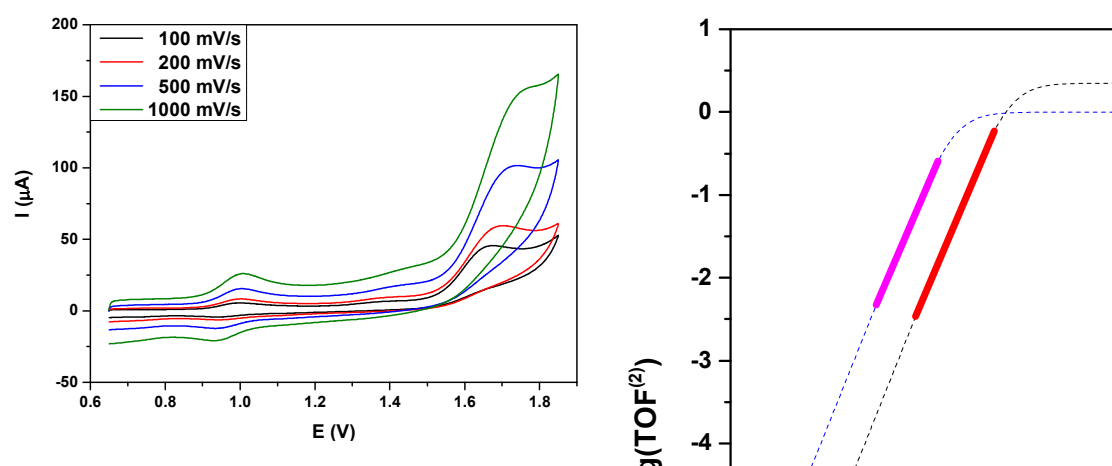
where E_{PQ}^0 is the standard potential for the catalysis-initiating redox couple (1.56 V for $3\mathbf{a}^{2+}$ and 1.64 V for $3\mathbf{b}^{2+}$, extracted from the DPVs in Figure S16), i is the current intensity in the presence of substrate, i_p^0 is the current intensity in the absence of substrate (we approximate this current to the current associated with the Ru(III)/Ru(II) couple), F is the faraday constant, v is the scan rate and R is $8.314 \text{ J mol}^{-1} \text{ K}^{-1}$. CVs of $3\mathbf{a}^{2+}$ at different scan rates (100 – 1000 mV/s) are shown in Figure 7 (left, top). k_{obs} can be extracted from the plot of i/i_p^0 vs. $1/\{1+\exp[(F/RT)(E_{\text{PQ}}^0-E)]\}$ as shown in Figure 7 (left, bottom) and in Figure S25 in the Supporting Information.

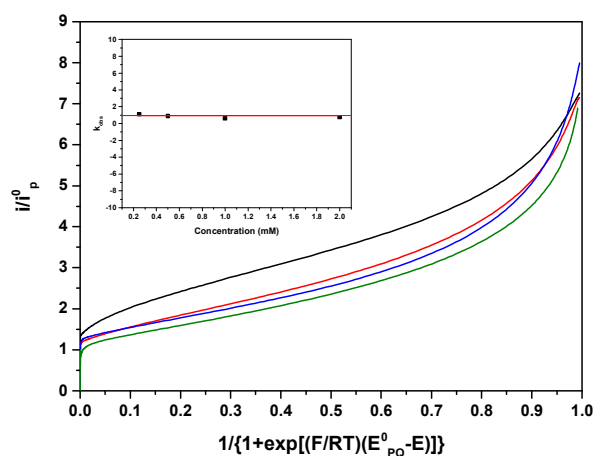
The largest slope at the very beginning of the catalytic process (which translates to the foot of the wave in the original CVs) gives a values of $k_{\text{obs}} = 1.00 \text{ s}^{-1}$ for $3\mathbf{a}^{2+}$ and 2.23 s^{-1} for $3\mathbf{b}^{2+}$. The relationship between the turnover frequency $\text{TOF}^{(2)}$ and the overpotential η , defined as the difference between the applied potential E and the thermodynamic potential of the catalyzed reaction E_{AC}^0 , in this case water oxidation, is governed by Equation 4 and plotted in Figure 7 (right).

$$\text{TOF}^{(2)} = \frac{k_{\text{obs}}}{1 + \exp \left[\frac{F}{RT} (E_{\text{PQ}}^0 - E_{\text{AC}}^0 - \eta) \right]} \quad (4)$$

The graph shows how the lower value of E_{PQ}^0 for $3a^{2+}$ translates in higher turnover frequencies when the overpotential is under 0.5 V. It should be noted that kinetic parameters for catalytic reactions derived from electrochemical measurements depend on various details of the experimental procedures, and values from different studies should be compared only with caution.²⁸

Figure 7. (Left, top) Background corrected CVs in H_2O/CF_3SO_3H (pH = 1.0) at 100-1000 mV/s scan rates. Black: 100 mV/s, red: 200 mV/s, blue: 500 mV/s, green: 1000 mV/s. (Left, bottom) Foot Of the Wave analysis plotting i/t_p^0 vs. $1/\{1+\exp[(F/RT)(E_{PQ}^0-E)]\}$ at each scan rate (same color code). Inset: plot of the different k_{obs} values extracted from the foot of the wave analysis at each scan rate. The red line represents the average k_{obs} value. (Right) Catalytic Taffel plots for $3a^{2+}$ (blue) and $3b^{2+}$ (black). The magenta and red line represent the scanned potentials.





Complexes **3a**²⁺ and **3b**²⁺ were tested for chemical water oxidation at pH = 1 with [(NH₄)₂Ce(NO₃)₆] (CAN). As shown in Figure S20, manometric measurements of both complexes show activity and the reaction is finished after 20 minutes. As expected by the electrochemical characterization, **3a**²⁺ is more reactive than the corresponding in isomer, yielding a 12.1 TON activity and a maximum TOF_i of $64.6 \times 10^{-3} \text{ s}^{-1}$, with an oxidative efficiency of 49%. On the other hand **3b**²⁺ exhibits lower activity (5.6 TON), TOF_i ($20.7 \times 10^{-3} \text{ s}^{-1}$) and oxidative efficiency (23%). To investigate the nature of the measured gas, on-line mass experiments were conducted under the same conditions as the manometry experiments, and the results are shown in Figure S20. The ratios O₂/CO₂ are in both cases favorable to oxygen: 9.1 for **3a**²⁺ and 2.9 for **3b**²⁺ (See Figure S20c). CO₂ production indicates oxidative degradation of the ligands, and is the probable responsible for the general low oxidative efficiency and in particular of the lower performances of the in isomer. The corrected values of the manometric experiments are consequently TON = 10.8 and TOF_i = $58.2 \times 10^{-3} \text{ s}^{-1}$ for **3a**²⁺ and TON = 4.2 and TOF_i = $15.4 \times 10^{-3} \text{ s}^{-1}$ for **3b**²⁺.

“This document is the Accepted Manuscript version of a Published Work that appeared in final form in Inorganic Chemistry, copyright © American Chemical Society after peer review and technical editing by the publisher. To access the final edited and published work see [insert ACS Articles on Request author- directed link to Published Work, see <http://pubs.acs.org/doi/abs/10.1021/acs.inorgchem.5b02260> .”

The higher generation of CO₂ by **3b**²⁺ could be attributed to a different impact of the electronic effects discussed through the present work on the two competing reactions: e.g. while favoring the water oxidation reaction for **3a**²⁺, they disfavor the competitive ligand oxidation reaction; and the opposite is true for **3b**²⁺.

Supporting Information content. Additional spectroscopic, electrochemical and catalytic experiments data. X-ray crystallographic data in CIF format. This material is available free of charge via the Internet at <http://pubs.acs.org>.

Acknowledgments. This research was supported by the Spanish Ministerio de Economía y Competitividad (MINECO) through projects CTQ-2013-49075-R, CTQ2014-52974-REDC, and by the EU COST actions CM1202 and CM1205. L. M. thanks “ICIQ-Foundation” for a Ph.D. grant. The Severo Ochoa Excellence Accreditation (SEV-2013-00319) is gratefully acknowledged.

REFERENCES

- (1) Tseng, H.-W.; Zong, R.; Muckerman, J. T.; Thummel, R., *Inorg. Chem.* **2008**, *47*, 11763-11773.
- (2) a) Zeng, Q.; Lewis, F. W.; Harwood, L. M.; Hartl, F., *Coord. Chem. Rev.* **2015**, *304–305*, 88-101; b) Kärkäs, M. D.; Verho, O.; Johnston, E. V.; Åkermark, B., *Chem. Rev.* **2014**; c) Limburg, B.; Bouwman, E.; Bonnet, S., *Coord. Chem. Rev.* **2012**, *256*, 1451-1467; d) Cao, R.; Lai, W.; Du, P., *Energy Environ. Sci.* **2012**, *5*, 8134-8157; e) Walden, A. G.; Miller, A. J. M., *Chem. Sci.* **2015**, *6*, 2405-2410; f) Honta, J.; Tajima, S.; Sato, T.; Saito, K.; Yui, T.; Yagi, M., *Journal of Photochemistry and Photobiology A: Chemistry* **2015**, *313*, 126-130; g) Yoshida, M.; Kondo, M.; Torii, S.; Sakai, K.; Masaoka, S., *Angew. Chem. Int. Ed.* **2015**, *54*, 7981-7984.
- (3) Concepcion, J. J.; Jurss, J. W.; Brennaman, M. K.; Hoertz, P. G.; Patrocinio, A. O. T.; Murakami Iha, N. Y.; Templeton, J. L.; Meyer, T. J., *Acc. Chem. Res.* **2009**, *42*, 1954-1965.
- (4) a) Wrzolek, P.; Schwalbe, M., *Eur. J. Inorg. Chem.* **2015**, *2015*, 4373-4378; b) Yan, L.; Zong, R.; Pushkar, Y., *J. Catal.* **2015**, *330*, 255-260; c) Pushkar, Y.; Moonshiram, D.; Purohit, V.; Yan, L.; Alperovich, I., *J. Am. Chem. Soc.* **2014**, *136*, 11938-11945.
- (5) Concepcion, J. J.; Jurss, J. W.; Templeton, J. L.; Meyer, T. J., *J. Am. Chem. Soc.* **2008**, *130*, 16462-16463.
- (6) a) Blakemore, J. D.; Schley, N. D.; Balcells, D.; Hull, J. F.; Olack, G. W.; Incarvito, C. D.; Eisenstein, O.; Brudvig, G. W.; Crabtree, R. H., *J. Am. Chem. Soc.* **2010**, *132*, 16017-16029; b)

Wasylenko, D. J.; Ganesamoorthy, C.; Borau-Garcia, J.; Berlinguette, C. P., *Chem. Commun.* **2011**, 47, 4249-4251.

(7) Wasylenko, D. J.; Ganesamoorthy, C.; Henderson, M. A.; Koivisto, B. D.; Osthoff, H. D.; Berlinguette, C. P., *J. Am. Chem. Soc.* **2010**, 132, 16094-16106.

(8) Maji, S.; López, I.; Bozoglian, F.; Benet-Buchholz, J.; Llobet, A., *Inorg. Chem.* **2013**, 52, 3591-3593.

(9) Yamazaki, H.; Hakamata, T.; Komi, M.; Yagi, M., *J. Am. Chem. Soc.* **2011**, 133, 8846-8849.

(10) Dubs, C.; Yamamoto, T.; Inagaki, A.; Akita, M., *Organometallics* **2006**, 25, 1344-1358.

(11) Evans, I. P.; Spencer, A.; Wilkinson, G., *J. Chem. Soc., Dalton Trans.* **1973**, 204-209.

(12) Ziessel, R.; Grosshenny, V.; Hissler, M.; Stroh, C., *Inorg. Chem.* **2004**, 43, 4262-4271.

(13) Data collection: APEX II, versions v2009.1-02 and v2013.4-1; Bruker AXS Inc.: Madison, WI, 2007.

(14) Data reduction: SAINT, versions V7.60A and V8.30c; Bruker AXS Inc.: Madison, WI, 2007.

(15) SADABS, V2008/1 and V2012/1; Bruker AXS Inc.: Madison, WI, 2001.

(16) Blessing, R., *Acta Crystallogr. Sect. A* **1995**, 51, 33-38.

(17) Sheldrick, G., *Acta Crystallogr. Sect. A* **2008**, 64, 112-122.

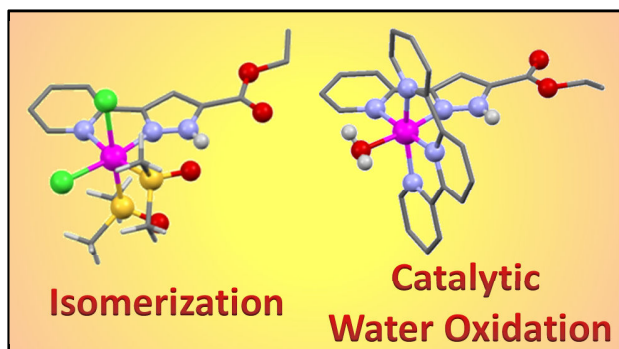
- (18) Sens, C.; Rodríguez, M.; Romero, I.; Llobet, A.; Parella, T.; Sullivan, B. P.; Benet-Buchholz, J., *Inorg. Chem.* **2003**, *42*, 2040-2048.
- (19) a) Planas, N.; Christian, G.; Roeser, S.; Mas-Marzá, E.; Kollipara, M.-R.; Benet-Buchholz, J.; Maseras, F.; Llobet, A., *Inorg. Chem.* **2012**, *51*, 1889-1901; b) Roeser, S.; Farràs, P.; Bozoglian, F.; Martínez-Belmonte, M.; Benet-Buchholz, J.; Llobet, A., *ChemSusChem* **2011**, *4*, 197-207; c) Farràs, P.; Maji, S.; Benet-Buchholz, J.; Llobet, A., *Chem. Eur. J.* **2013**, *19*, 7162-7172; d) Romero, I.; Rodríguez, M.; Llobet, A.; Collomb-Dunand-Sauthier, M.-N.; Deronzier, A.; Parella, T.; Stoeckli-Evans, H., *J. Chem. Soc., Dalton Trans.* **2000**, 1689-1694.
- (20) Mognon, L.; Benet-Buchholz, J.; Rahaman, S. M. W.; Bo, C.; Llobet, A., *Inorg. Chem.* **2014**, *53*, 12407-12415.
- (21) Sens, C.; Rodríguez, M.; Romero, I.; Llobet, A.; Parella, T.; Benet-Buchholz, J., *Inorg. Chem.* **2003**, *42*, 8385-8394.
- (22) Roeser, S.; Maji, S.; Benet-Buchholz, J.; Pons, J.; Llobet, A., *Eur. J. Inorg. Chem.* **2013**, *2013*, 232-240.
- (23) Nicholson, R. S.; Shain, I., *Anal. Chem.* **1964**, *36*, 706-723.
- (24) Silva, D. O.; Toma, H. E., *Can. J. Chem.* **1994**, *72*, 1705-1708.
- (25) Benet-Buchholz, J.; Comba, P.; Llobet, A.; Roeser, S.; Vadivelu, P.; Wiesner, S., *Dalton Trans.* **2010**, *39*, 3315-3320.
- (26) Lever, A. B. P., *Inorg. Chem.* **1990**, *29*, 1271-1285.

“This document is the Accepted Manuscript version of a Published Work that appeared in final form in *Inorganic Chemistry*, copyright © American Chemical Society after peer review and technical editing by the publisher. To access the final edited and published work see [insert ACS Articles on Request author- directed link to Published Work, see <http://pubs.acs.org/doi/abs/10.1021/acs.inorgchem.5b02260> .”

(27) Costentin, C.; Drouet, S.; Robert, M.; Savéant, J.-M., *J. Am. Chem. Soc.* **2012**, *134*, 11235-11242.

(28) Rountree, E. S.; McCarthy, B. D.; Eisenhart, T. T.; Dempsey, J. L., *Inorg. Chem.* **2014**, *53*, 9983-10002.

For Table of Contents Only



A family of Ru complexes containing a pyridyl-pyrazolate ligand have been prepared and thoroughly studied by spectroscopic and electrochemical methods. The Ru-dmso complex undergoes dmso linkage isomerization upon oxidation of Ru(II) to Ru(III) whereas the *in*- and *out*-Ru-aqua isomeric complexes behave as water oxidation catalysts.